

# 1 **Impact of textural patterns on rock weathering rates and size distribution of** 2 **weathered grains**

3 **Yoni Israeli<sup>1</sup>, Eyal Salhov<sup>1</sup>, and Simon Emmanuel<sup>1</sup>**

4 <sup>1</sup>The Institute of Earth Sciences, The Hebrew University of Jerusalem, Edmond J. Safra Campus,  
5 Givat Ram, Jerusalem 91904, Israel.

6 Corresponding author: Yoni Israeli ([israeli.yoni@gmail.com](mailto:israeli.yoni@gmail.com))

## 7 **Highlights**

- 8 • Numerical model simulating chemical weathering and grain detachment in rocks with  
9 different textural patterns.
- 10 • Weathering rate increases with increasing density of discontinuities.
- 11 • Mean size of detached fragments decreases with increasing tortuosity of the textural  
12 patterns.

## 13 **Abstract**

14 Rock texture has a critical influence on the way rocks weather. The most important textural  
15 factors affecting weathering are grain size and the presence of cracks and stylolites. These  
16 discontinuities operate as planes of mechanical weakness at which chemical weathering is  
17 enhanced. However, it is unclear how different rock textures impact weathering rates and the size  
18 of weathered grains. Here, we use a numerical model to simulate weathering of rocks possessing  
19 grain boundaries, cracks, and stylolites. We ran simulations with either synthetic or natural patterns  
20 of discontinuities. We found that for all patterns, weathering rates increase with discontinuity  
21 density. When the density was  $< \sim 25\%$ , the weathering rate of synthetic patterns followed the order:  
22 grid > honeycomb > Voronoi > brick-wall. For higher values, all weathering rates were similar. We  
23 also found that weathering rates decreased as the tortuosity of the pattern increased. Moreover, we  
24 show that textural patterns strongly impact the size distributions of detached grains. Rocks with an  
25 initial monomodal grain size distribution produce weathered fragments that are normally  
26 distributed. In contrast, rocks with an initial log-normal size distribution produce weathered grains

27 that are log-normally distributed. For the natural patterns, weathering produced lower modality  
28 distributions.

29 **Keywords:** Chemical Weathering, Grain Size, Fractures, Stylolites, Physical weathering,  
30 Dissolution.

## 31 **1 Introduction**

32 Both natural and anthropogenic processes are affected by the rate at which rocks weather.  
33 Weathering rates impact the development of landscapes, the formation of soils, the fluid flow in  
34 aquifers and petroleum reservoirs, and the durability of buildings and monuments [1-3]. In  
35 addition, weathering rate plays a significant role in the global carbon cycle [4, 5], regulating  
36 atmospheric CO<sub>2</sub> on geological time scales [6]. Artificially accelerated weathering has even been  
37 suggested as a way of mitigating present-day anthropogenic carbon emissions [5, 7-9].

38 Weathering rates are affected by both chemical and physical mechanisms. Rocks  
39 comprising minerals that are susceptible to chemical processes, such as dissolution, oxidation, and  
40 hydrolysis are expected to weather more rapidly than rocks comprising inert minerals [10-15]. In  
41 addition, physical processes such as frost shattering, thermal expansion, and unloading [16-20] can  
42 induce fracturing that causes mechanical weathering. Complicating matters further, chemical and  
43 physical processes are often coupled [10, 21-24]. As the density of cracks increases, more mineral  
44 surfaces are exposed to chemical reactions. At the same time, chemical dissolution along these  
45 cracks increases the overall porosity and weakens the rock mechanically [25, 26], accelerating  
46 physical weathering.

47 At the microscopic scale, weathering rates are affected by discontinuities that include  
48 crystalline defects, crystal edges and corners, and grain boundaries [27, 28]. For example, the rate  
49 of dissolution along the edges and corners of a calcite spar was measured to be 1.7-3.6 faster than  
50 of the mineral face [29]. In polycrystalline rocks, grain boundaries were found to be an order of  
51 magnitude more reactive than the bulk mineral [30-32]. In studies focused on rock weathering at  
52 the submicron scale, enhanced dissolution at grain boundaries was shown to cause the mechanical  
53 detachment of particles into the fluid phase [33-36]. Such chemo-mechanical rock weathering was  
54 observed in micritic limestone, [37], however, particle detachment can occur in various types of  
55 rocks with larger grain sizes and different mineral compositions [37-39].

56 At macroscopic scales, rock weathering is accelerated by other types of discontinuities  
57 such as cracks, joints, fractures, and stylolites [26, 40], which operate as planes of mechanical  
58 weakness and enhanced chemical weathering [20, 41, 42]. For example, Røyne et al. [21] showed  
59 that outcrop weathering is controlled by continual fracturing and production of surface area, which  
60 allows fluids to penetrate deeper into the rock and accelerate weathering rates.

61 While discontinuities are known to enhance weathering rates, the impact of different  
62 patterns and textures remains unclear. Discontinuities often show spatial ordering and fractal  
63 behavior [43-47], appearing in several superimposed networks reflecting the geological history of  
64 the rocks [26, 48]. Typical patterns include conjugated sets of fractures, grid and ladder-like  
65 patterns, polygonal joints, and columnar joints [26, 48, 49]. Furthermore, similar patterns can have  
66 different levels of connectivity depending on the spacing, orientation, length, and density of the  
67 discontinuities. The convolution of these factors can be represented by tortuosity, which is a  
68 measure of the geometric complexity of the pathways by which reactive fluids penetrate the rock.  
69 High tortuosity is expected to lead to reduced weathering rates, while low tortuosity could intensify  
70 weathering.

71 Here, we develop a cellular automaton model that simulates coupled chemo-mechanical  
72 weathering processes of rocks with different kinds of discontinuities and textural patterns.  
73 Specifically, we analyze the impact of the density and tortuosity of the discontinuities on the  
74 weathering rate. In addition, we examine how these parameters impact the size distribution of  
75 weathered rock fragments. We also discuss the implications for both surface and subsurface  
76 processes including soil and regolith production.

## 77 **2 Methods and data**

### 78 2.1 Model structure

79 To simulate the effects of chemo-mechanical weathering on rocks with different textures  
80 and grain size distributions, we used a model based on that described by Israeli and Emmanuel  
81 [39]. A 2-D cross-section of the rock was represented using a domain with 560\*420 elements.  
82 Each element represented either a solid mineral, a discontinuity, or a fluid phase and is assigned a  
83 characteristic value.

84 In the simulations, chemical weathering only occurs in elements neighboring the fluid  
85 phase. In every time step, the probability that an element will dissolve depends both on the  
86 characteristic value of the element and the number of neighboring fluid elements. The dissolved  
87 elements are then reassigned as a fluid phase, and the domain is scanned for interconnected  
88 elements that are fully surrounded by fluid. These surrounded elements are considered to be  
89 detached physically and their elements are also reassigned to the fluid phase (Figure 1).

90 The discontinuities in the model are intended to represent grain boundaries, joints, cracks,  
91 or stylolites which are partially filled with cement. Thus, the discontinuities have an intrinsic  
92 strength that binds the rock together but they also dissolve more rapidly than the bulk rock, and  
93 this effect is included in the model.

94 The data from every simulation was saved as an object comprised of all the information  
95 from the simulation, including the rock's initial properties and the dynamic properties of the rock  
96 in every step. These properties include an image of the rock in every step, a list of pixels that were  
97 dissolved, location, and dimensions of detached fragments in every step. Using this object-oriented  
98 approach in Matlab™, each simulation takes several minutes on a standard PC and the data is  
99 uploaded into a MySQL database facilitating analysis of the datasets.

## 100 2.2 Patterns of discontinuities

101 In our model, we used two kinds of discontinuity patterns: synthetic and natural (Figure 2).  
102 Four different synthetic patterns were tested: (i) regular grid jointing; (ii) brick wall jointing; (iii)  
103 hexagonal jointing, simulating columnar patterns common in basalts; (iv) Voronoi tessellation,  
104 representing a coarse-grained crystalline rock. Weathering was also simulated for 4 natural rock  
105 patterns, obtained by binarization of outcrop images: (i) diagonal cracks; (ii) orthogonal cracks;  
106 (iii) stylolites oriented perpendicular to the weathering front; (iv) stylolites oriented sub-parallel  
107 to the weathering front. The crack patterns are taken from two locations: drone images from  
108 McDonald limestone in Scotland [44] and a limestone outcrop at the south margin of the Bristol  
109 Channel Basin, UK [50]. The stylolite patterns are derived from images of carbonate rocks from  
110 Israel, reported by Laronne Ben-Itzhak et al. [51].

## 111 2.3 Model calculations

112 In the initial state of our simulations, we define a grain or block as a region bounded by  
113 discontinuities. We also define the discontinuity density as the proportion of discontinuity pixels

114 in the domain. For natural rock patterns in our simulations, this varies in the range 2% to 30%,  
115 while for synthetic patterns this varies from 7% to 40%. For natural patterns, different values of  
116 discontinuity density were obtained by cropping the images. In simulations using synthetic  
117 patterns, discontinuity density is controlled by the number of grains in the domain: increasing the  
118 number of grains increases the discontinuity density.

119 Six different realizations were carried out for each pattern type, and a total of ~6000  
120 simulations were completed. At each step, we calculated the number of elements removed by  
121 chemical weathering and by mechanical weathering. The dimensions and locations of each  
122 detached grain were recorded. The available reactive surface in every time step was also calculated,  
123 based on the location of the pixels that neighbor the reactive fluid. The data were then analyzed to  
124 assess the weathering rate and the grain size distribution of the detached fragments. When  
125 calculating the grain size distributions, we only considered detached clusters larger than 10 pixels,  
126 and the amplitude of each size bin represents the cumulative number of pixels of the individual  
127 grains within the bin. This approach is similar, but not identical, to grain size distributions  
128 determined by mass in unconsolidated sediments and soils [52, 53].

129 For our model domains, we also calculated the tortuosity of the discontinuity patterns.  
130 There are several different definitions of tortuosity [54], and here, we adapted the definition of  
131 Cooper et al. [55] based on the convolution of diffusive transport flow paths:

$$132 \quad (1) \quad \tau = \epsilon \frac{D}{D^{\text{eff}}},$$

133 where  $\epsilon$  is the discontinuity density,  $D$  is the intrinsic diffusivity of the discontinuity network,  
134 while  $D^{\text{eff}}$  is the effective diffusivity through the bulk rock. We used the Tau Factor Matlab™  
135 application [55] to calculate the tortuosity based on our 2D images.

136

### 137 **3 Results and discussion**

#### 138 **3.1 Impact of discontinuity density on rock weathering rates**

139 For all the rock patterns we tested, we found weathering rates to increase as the  
140 discontinuity density increased (Figure 3). This result is not surprising since the dissolution rate  
141 along the discontinuities is more rapid than the dissolution rate of the bulk rock. Moreover, this is  
142 consistent with field and experimental observations of weathering rates in fractured rocks [20, 21].

143 Our simulations also show that the type of discontinuity pattern has a significant impact on  
144 weathering rates (Figure 3), particularly at discontinuity densities  $<25\%$ . For the synthetic patterns,  
145 at any given value of discontinuity density, the rates followed the order: grid  $>$  honeycomb  $>$   
146 Voronoi  $>$  brick wall. In natural rock patterns, the order was less clear, although weathering in  
147 orthogonal cracks was faster than in diagonal cracks, and weathering in perpendicular stylolites  
148 was faster than in parallel stylolites. In addition, synthetic patterns generally weathered faster than  
149 natural rock patterns. This is probably due to the irregular nature of natural patterns and their  
150 inherently lower connectivity.

151 At discontinuity densities  $>25\%$ , the weathering rates of all the patterns begin to converge.  
152 This may be because at low discontinuity densities, the tortuosity of the pathways and their low  
153 connectivity acts as a limiting factor. As the discontinuity density increases, connectivity is  
154 expected to increase, facilitating the advance of the weathering front. Although the discontinuity  
155 density is a critical parameter in determining weathering rates, our results suggest that additional  
156 parameters related to the geometry of the patterns are also likely to impact the way rocks weather.  
157 Specifically, for patterns in which the pathways are highly tortuous and poorly connected, rates  
158 are expected to be slower.

### 159 3.2 Impact of tortuosity on weathering rates

160 In the simulations of synthetic rocks, each pattern type showed a decrease in weathering  
161 rate with increasing tortuosity (Figure 4a). Moreover, the rates grouped into two distinct trends:  
162 (i) grid and brick wall, and (ii) honeycomb and Voronoi. This is probably due to the similarity in  
163 the geometry of the patterns within each trend. By contrast, for natural rock patterns, there is no  
164 clear dependence of weathering rate on tortuosity for individual pattern types (Figure 4b). This  
165 could be related to the irregularity and anisotropy of discontinuities in natural patterns, which can  
166 cause patterns with identical tortuosities to behave differently. In addition, the widely varying  
167 discontinuity densities in the natural patterns could also mask the apparent impact of tortuosity.

168 To isolate the impact of tortuosity, we conducted a numerical experiment with simulations  
169 of synthetic patterns in which tortuosity changed systematically while maintaining the same level  
170 of discontinuity density (Figure 5). Starting with a regular grid, we introduced an offset in  
171 alternating layers to create brick wall patterns, which increased the tortuosity. In this method, the  
172 tortuosity varied from 1.95-2.75. In each offset, we ran six simulations with 3 different initial grain  
173 sizes: 2160, 234, and 108 pixels.

174 Our results show a near-linear decrease in the weathering rate as the tortuosity increases  
175 from 1.95 to 2.75 (Figure 6) for all the three grain sizes tested. Overall, the reduction in rate was  
176 33%, 21%, and 27% for the 2160, 234, and 108 grain size simulations, respectively. This  
177 significant effect means that in addition to mineralogy and grain size, the tortuosity of the  
178 discontinuity pattern is likely to be a critical factor in determining the weathering rate in real rocks.

### 179 3.3 Impact of discontinuity density and tortuosity on size of detached grains:

180 We found the mean detached grain size decreases non-linearly with increasing  
181 discontinuity density for both synthetic and natural patterns (Figure 7). For the synthetic patterns,  
182 the detachment grain size drops by approximately 90% as the discontinuity density increases from  
183 8% to 25% (Figure 7a). For natural patterns, there is a significant level of variability and the trend  
184 is far less clear (Figure 7b). This is most likely a result of the differences between the initial  
185 conditions in the synthetic patterns and those in the natural patterns: in the synthetic patterns, the  
186 initial grain sizes are similar for any given discontinuity density, while in natural patterns, the  
187 initial grain size varies significantly.

188 The overall reduction of the mean detached fragment size with increasing discontinuity  
189 density is caused by two factors. The first is that increasing discontinuity density leads to a  
190 reduction in the initial grain size, which results in smaller detached grains. The second is that as  
191 the discontinuity density increases, the chemical weathering rate also increases, causing the grains  
192 to undergo more dissolution prior to detachment.

193 To test if tortuosity plays a role in the size of detached grains, we analyzed the results of  
194 the offset experiment described in Section 3.2 and found that the mean detachment size decreases  
195 with increasing tortuosity (Figure 8). This is because in patterns with higher tortuosity, chemical  
196 dissolution has longer time to act and reduce the size of the grains prior to detachment. This effect  
197 can be seen in the simulation snapshots in Figure 5: detaching grains in the grid simulation are  
198 larger than the detaching grains in the offset simulations.

### 199 3.4 Impact of textural patterns on the size distribution of weathered grains

200 In all the rock patterns we tested, the grain size distribution of detached blocks was  
201 influenced by the rock textural patterns. For the synthetic patterns possessing an *initial* uniform  
202 grain size (grid, honeycomb, brick-wall), the *detached* grains showed a normal size distribution

203 (Figure 9 a-c). By contrast, for Voronoi patterns, the detached grain size distribution was log-  
204 normal, similar to the initial grain size distribution (Figure 9d). For the natural rock patterns we  
205 tested (stylolites and cracks), the initial block size distributions were multimodal. However, the  
206 size distribution of the detached fragments showed reduced modality (Figure 10). Our results are  
207 consistent with the findings of Palomares et al. [56] who showed that rocks with similar initial  
208 grain sizes fragment mainly along their uniformly distributed discontinuities, thus providing grains  
209 of uniform size, in contrast to rocks with anisotropic fabrics that do not disintegrate uniformly.

210 Grain size distributions of weathered grains strongly influence soil permeability and soil  
211 erosion [57]. Soils with a wide range of grain sizes are less permeable and erode less readily than  
212 soils with uniform grain size distributions [57]. Thus, we expect rocks with initial grid-like, or  
213 honeycomb discontinuity patterns to produce relatively uniform grain size distributions that form  
214 soils with higher permeabilities. By contrast, rocks with stylolites and cracks might be expected to  
215 produce soils that form impermeable layers.

216 Although there is significant variability, the grain size distribution of many soils and  
217 sediments often has a log-normal distribution [58, 59]. In our simulations, the only pattern that  
218 weathered into fragments with log-normal distributions is the Voronoi pattern. These patterns are  
219 common in the polycrystalline rocks that provide much of the weathered material to sediments,  
220 and it is likely that the log-normal distribution in sediments is influenced by the initial grain size  
221 distribution of the weathered rock. However, transport processes also strongly affect the size  
222 distributions of sediments, [54], and we therefore expect the discontinuity patterns to have the  
223 strongest impact on the distribution of sediments that are relatively close to the source rock, such  
224 as in fluvial fans.

225

## 226 **4 Conclusions**

227 In this study, we used a numerical model that incorporates both chemical and mechanical  
228 weathering to investigate the impact of rock texture on weathering rate and the size of detached  
229 grains. Our results indicate that the weathering rate increases with increasing densities of  
230 discontinuities in the rock. We also found that increasing the tortuosity of the patterns lead to  
231 decreasing weathering rates. Moreover, we found a strong impact of texture on the detached grain  
232 size distribution, and that higher discontinuity densities leads to smaller detached blocks. This has  
233 practical implications for risk assessment near cliffs or stone edifices: rocks containing stylolites

234 with spacings of several centimeters could present less of a risk than rocks containing fractures  
235 with spacings of tens of centimeters.

236 The model we present here is a preliminary attempt to simulate the combined effects of  
237 chemical and mechanical weathering, and we can identify some limitations to our approach. Our  
238 simulations compare textures of different scales: the individual grains comprising a rock are often  
239 micrometer or millimeter in scale, while joints and stylolites are often present at the centimeter  
240 and meter-scale. Moreover, the time and spatial scales in the model are at present arbitrary, which  
241 severely limits its predictive power. Calibrating the model, however, requires reliable field data,  
242 which are difficult to obtain because of the long time scales associated with weathering. Future  
243 work that focuses on improving the model by comparison with field-based measurements could  
244 provide solutions to some of these challenges.

## 245 **Acknowledgments and Data**

246 This research was supported by student scholarships from the Israeli Water Authority, the  
247 Rieger Foundation, and the Hebrew University Advanced School of Environmental Studies. The  
248 Israel Science Foundation is thanked for their generous support. The dataset for this research is  
249 publicly available in the Mendeley Data repository at DOI: <http://dx.doi.org/10.17632/v4jw2d9rbm.1>  
250 [60].

## 251 **References**

- 252 [1] Brantley SL. Kinetics of Mineral Dissolution. In: Brantley SL, Kubicki JD, White AF, editors. Kinetics of  
253 Water-Rock Interaction. New York, NY: Springer New York, 2008. p. 151-210.
- 254 [2] Dixon JL, Hartshorn AS, Heimsath AM, DiBiase RA, Whipple KX. Chemical weathering response to tectonic  
255 forcing: A soils perspective from the San Gabriel Mountains, California. *Earth and Planetary Science Letters*.  
256 2012;323-324(40-9).
- 257 [3] Wilson MJ. Weathering of the primary rock-forming minerals: processes, products and rates. *claymin*.  
258 2004;39(3):233.
- 259 [4] Li G, Elderfield H. Evolution of carbon cycle over the past 100 million years. *Geochimica et Cosmochimica*  
260 *Acta*. 2013;103(11-25).
- 261 [5] Torres MA, West AJ, Clark KE, Paris G, Bouchez J, Ponton C, et al. The acid and alkalinity budgets of  
262 weathering in the Andes–Amazon system: Insights into the erosional control of global biogeochemical cycles. *Earth*  
263 *and Planetary Science Letters*. 2016;450(381-91).
- 264 [6] Them TR, Gill BC, Selby D, Gröcke DR, Friedman RM, Owens JD. Evidence for rapid weathering response to  
265 climatic warming during the Toarcian Oceanic Anoxic Event. *Scientific Reports*. 2017;7(1):5003.
- 266 [7] Beerling DJ, Kantzas EP, Lomas MR, Wade P, Eufrazio RM, Renforth P, et al. Potential for large-scale CO<sub>2</sub>  
267 removal via enhanced rock weathering with croplands. *Nature*. 2020;583(7815):242-8.
- 268 [8] Strefler J, Amann T, Bauer N, Kriegler E, Hartmann J. Potential and costs of carbon dioxide removal by  
269 enhanced weathering of rocks. *Environmental Research Letters*. 2018;13(3):034010.

270 [9] Xu Z, Liu C-Q. Water geochemistry of the Xijiang basin rivers, South China: Chemical weathering and CO<sub>2</sub>  
271 consumption. *Applied Geochemistry*. 2010;25(10):1603-14.

272 [10] Buss HL, Sak PB, Webb SM, Brantley SL. Weathering of the Rio Blanco quartz diorite, Luquillo Mountains,  
273 Puerto Rico: Coupling oxidation, dissolution, and fracturing. *Geochimica et Cosmochimica Acta*. 2008;72(18):4488-  
274 507.

275 [11] Critelli T, Marini L, Schott J, Mavromatis V, Apollaro C, Rinder T, et al. Can the dissolution rates of individual  
276 minerals be used to describe whole rock dissolution? EGU General Assembly Conference Abstracts2014.

277 [12] Goldich SS. A Study in Rock-Weathering. *The Journal of Geology*. 1938;46(1):17-58.

278 [13] Maher K, Steefel CI, White AF, Stonestrom DA. The role of reaction affinity and secondary minerals in  
279 regulating chemical weathering rates at the Santa Cruz Soil Chronosequence, California. *Geochimica et*  
280 *Cosmochimica Acta*. 2009;73(10):2804-31.

281 [14] Nesbitt HW, Young GM. Formation and Diagenesis of Weathering Profiles. *The Journal of Geology*.  
282 1989;97(2):129-47.

283 [15] White AF, Buss HL. Natural Weathering Rates of Silicate Minerals. *Treatise on Geochemistry (Second*  
284 *Edition)*, Elsevier, Oxford. 2014:115-55.

285 [16] Matsuoka N, Murton J. Frost weathering: recent advances and future directions. *Permafrost and Periglacial*  
286 *Processes*. 2008;19(2):195-210.

287 [17] Park J, Hyun CU, Park HD. Changes in microstructure and physical properties of rocks caused by artificial  
288 freeze–thaw action. *Bulletin of Engineering Geology and the Environment*. 2015;74(2):555-65.

289 [18] Hall K. The role of thermal stress fatigue in the breakdown of rock in cold regions. *Geomorphology*.  
290 1999;31(1):47-63.

291 [19] Molnar P. Interactions among topographically induced elastic stress, static fatigue, and valley incision. *Journal*  
292 *of Geophysical Research: Earth Surface*. 2004;109(F2).

293 [20] Eppes M-C, Keanini R. Mechanical weathering and rock erosion by climate-dependent subcritical cracking.  
294 *Rev Geophys*. 2017;55(2):470-508.

295 [21] Røyne A, Jamtveit B, Mathiesen J, Malthe-Sørenssen A. Controls on rock weathering rates by reaction-induced  
296 hierarchical fracturing. *Earth and Planetary Science Letters*. 2008;275(3):364-9.

297 [22] Anderson SP, Blum J, Brantley SL, Chadwick O, Chorover J, Derry LA, et al. Proposed initiative would study  
298 Earth's weathering engine. *Eos, Transactions American Geophysical Union*. 2004;85(28):265-9.

299 [23] Larsen IJ, Almond PC, Eger A, Stone JO, Montgomery DR, Malcolm B. Rapid Soil Production and Weathering  
300 in the Southern Alps, New Zealand. *Science*. 2014;343(6171):637-40.

301 [24] Fletcher R, Buss H, Brantley S. A spheroidal weathering model coupling porewater chemistry to soil  
302 thicknesses during steady-state denudation. *Earth and Planetary Science Letters*. 2006;244(1-2):444-57.

303 [25] Brantley SL, Evans B, Hickman SH, Crerar DA. Healing of microcracks in quartz: Implications for fluid flow.  
304 *Geology*. 1990;18(2):136-9.

305 [26] Singhal BBS, Gupta RP. Fractures and Discontinuities. In: Singhal BBS, Gupta RP, editors. *Applied*  
306 *Hydrogeology of Fractured Rocks: Second Edition*. Dordrecht: Springer Netherlands, 2010. p. 13-33.

307 [27] Holdren GR, Speyer PM. Reaction rate-surface area relationships during the early stages of weathering. II. Data  
308 on eight additional feldspars. *Geochimica et Cosmochimica Acta*. 1987;51(9):2311-8.

309 [28] Trindade Pedrosa E, Kurganskaya I, Fischer C, Luttge A. A Statistical Approach for Analysis of Dissolution  
310 Rates Including Surface Morphology. *Minerals*. 2019;9(8):458.

311 [29] Noiriel C, Oursin M, Saldi G, Haberthür D. Direct Determination of Dissolution Rates at Crystal Surfaces  
312 Using 3D X-ray Microtomography. *ACS Earth and Space Chemistry*. 2019;3(1):100-8.

313 [30] Bray AW, Oelkers EH, Bonneville S, Wolff-Boenisch D, Potts NJ, Fones G, et al. The effect of pH, grain size,  
314 and organic ligands on biotite weathering rates. *Geochimica et Cosmochimica Acta*. 2015;164(127-45).

315 [31] Emmanuel S. Mechanisms influencing micron and nanometer-scale reaction rate patterns during dolostone  
316 dissolution. *Chemical Geology*. 2014;363(262-9).

317 [32] Jonas L, John T, King HE, Geisler T, Putnis A. The role of grain boundaries and transient porosity in rocks as  
318 fluid pathways for reaction front propagation. *Earth and Planetary Science Letters*. 2014;386(64-74).

319 [33] Emmanuel S, Levenson Y. Limestone weathering rates accelerated by micron-scale grain detachment. *Geology*.  
320 2014;42(9):751-4.

321 [34] Fischer C, Luttge A. Beyond the conventional understanding of water–rock reactivity. *Earth and Planetary*  
322 *Science Letters*. 2017;457(100-5).

323 [35] Krklec K, Domínguez-Villar D, Carrasco RM, Pedraza J. Current denudation rates in dolostone karst from  
324 central Spain: Implications for the formation of unroofed caves. *Geomorphology*. 2016;264(1-11).

325 [36] Silveira FA, Aarão Reis FDA. Detachment of non-dissolved clusters and surface roughening in solid  
326 dissolution. *Electrochimica Acta*. 2013;111(1-8).

327 [37] Levenson Y, Emmanuel S. Quantifying micron-scale grain detachment during weathering experiments on  
328 limestone. *Geochimica et Cosmochimica Acta*. 2016;173(86-96).

329 [38] Krklec K, Marjanac T, Perica D. Analysis of "standard" (Lipica) limestone tablets and their weathering by  
330 carbonate staining and SEM imaging, a case study on the Vis Island, Croatia. *Acta Carsologica*. 2013;42(1):135-42.

331 [39] Israeli Y, Emmanuel S. Impact of grain size and rock composition on simulated rock weathering. *Earth Surf*  
332 *Dynam*. 2018;6(2):319-27.

333 [40] Heap M, Reuschlé T, Baud P, Renard F, Iezzi G. The permeability of stylolite-bearing limestone. *Journal of*  
334 *Structural Geology*. 2018;116(81-93).

335 [41] Lei Q, Latham J-P, Tsang C-F. The use of discrete fracture networks for modelling coupled geomechanical and  
336 hydrological behaviour of fractured rocks. *Computers and Geotechnics*. 2017;85(151-76).

337 [42] Pacheco FAL, Alencão AMP. Role of fractures in weathering of solid rocks: narrowing the gap between  
338 laboratory and field weathering rates. *Journal of Hydrology*. 2006;316(1):248-65.

339 [43] Ghosh A, Daemen JJK. Fractal characteristics of rock discontinuities. *Engineering Geology*. 1993;34(1):1-9.

340 [44] Healy D, Rizzo RE, Cornwell DG, Farrell NJ, Watkins H, Timms NE, et al. FracPaQ: A MATLAB™ toolbox  
341 for the quantification of fracture patterns. *Journal of Structural Geology*. 2017;95(1-16).

342 [45] Jafari A, Babadagli T. Estimation of equivalent fracture network permeability using fractal and statistical  
343 network properties. *Journal of Petroleum Science and Engineering*. 2012;92-93(110-23).

344 [46] Liu R, Jiang Y, Li B, Wang X. A fractal model for characterizing fluid flow in fractured rock masses based on  
345 randomly distributed rock fracture networks. *Computers and Geotechnics*. 2015;65(45-55).

346 [47] Babadagli T. Unravelling transport in complex natural fractures with fractal geometry: A comprehensive review  
347 and new insights. *Journal of Hydrology*. 2020;587(124937).

348 [48] Josnin J-Y, Jourde H, Pascal F, Bidaux P. A three-dimensional model to simulate joint networks in layered  
349 rocks. *Canadian Journal of Earth Sciences*. 2011;39(1443-55).

350 [49] Chan MA, Yonkee WA, Netoff DI, Seiler WM, Ford RL. Polygonal cracks in bedrock on Earth and Mars:  
351 Implications for weathering. *Icarus*. 2008;194(1):65-71.

352 [50] Belayneh M, Cosgrove JW. Fracture-pattern variations around a major fold and their implications regarding  
353 fracture prediction using limited data: an example from the Bristol Channel Basin. *Geological Society, London,*  
354 *Special Publications*. 2004;231(1):89-102.

355 [51] Laronne Ben-Itzhak L, Aharonov E, Karcz Z, Kaduri M, Toussaint R. Sedimentary stylolite networks and  
356 connectivity in limestone: Large-scale field observations and implications for structure evolution. *Journal of*  
357 *Structural Geology*. 2014;63(106-23).

358 [52] Blott SJ, Pye K. GRADISTAT: a grain size distribution and statistics package for the analysis of  
359 unconsolidated sediments. *Earth surface processes and Landforms*. 2001;26(11):1237-48.

360 [53] Konert M, Vandenberghe J. Comparison of laser grain size analysis with pipette and sieve analysis: a solution  
361 for the underestimation of the clay fraction. *Sedimentology*. 1997;44(3):523-35.

362 [54] Hunt AG, Sahimi M. Flow, Transport, and Reaction in Porous Media: Percolation Scaling, Critical-Path  
363 Analysis, and Effective Medium Approximation. *Rev Geophys*. 2017;55(4):993-1078.

364 [55] Cooper SJ, Bertei A, Shearing PR, Kilner JA, Brandon NP. TauFactor: An open-source application for  
365 calculating tortuosity factors from tomographic data. *SoftwareX*. 2016;5(203-10).

366 [56] Palomares M, Arribas J, Johnsson MJ, Basu A. Modern stream sands from compound crystalline sources:  
367 Composition and sand generation index. *Processes Controlling the Composition of Clastic Sediments: Geological*  
368 *Society of America*, 1993. p. 0.

369 [57] Cohen S, Willgoose G, Svoray T, Hancock G, Sela S. The effects of sediment transport, weathering, and  
370 aeolian mechanisms on soil evolution. *Journal of Geophysical Research: Earth Surface*. 2015;120(2):260-74.

371 [58] Gardner W. Representation of soil aggregate-size distribution by a logarithmic-normal distribution1, 2. *Soil*  
372 *Science Society of America Journal*. 1956;20(2):151-3.

373 [59] Wagner LE, Ding D. Representing aggregate size distributions as modified lognormal distributions.  
374 *Transactions of the ASAE*. 1994;37(3):815-21.

375 [60] Israeli Y. Dataset of Israeli et al 2020-Impact of textural patterns on rock weathering rates and size distribution  
376 of weathered grains. In: *Data M*, editor. V1 ed2020.

Figure 1:

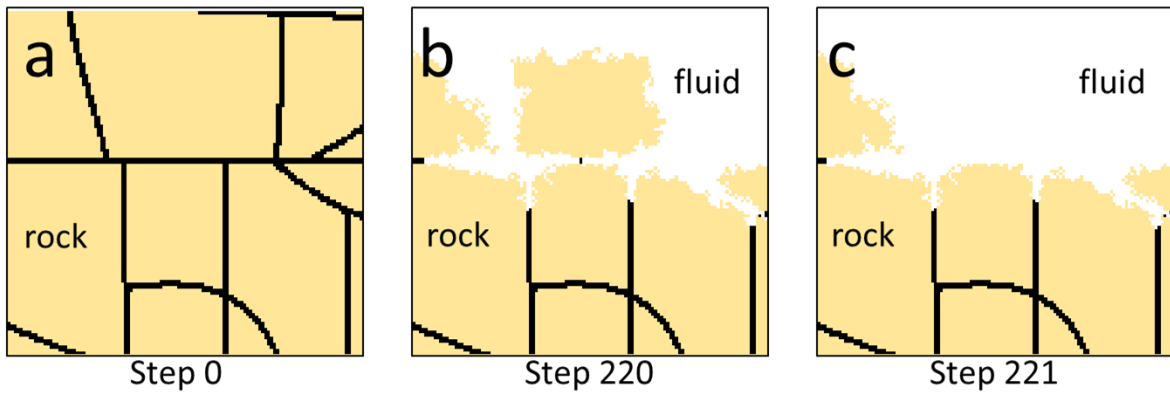


Figure 1. Simulation of fluid-rock interaction. The bulk rock components are marked in yellow, rock discontinuities in black, and fluid in white. Cross sections of the rock are shown at 3 stages of the simulation: (a) initial state; (b) Step 220 and (c) Step 221. Chemical weathering dissolves the rock minerals slower than the discontinuities between rock clusters. When a cluster is surrounded by fluid it detaches from the surface and is removed from the simulation. Note that the black discontinuities dissolve more rapidly than the bulk rock.

Figure 2.

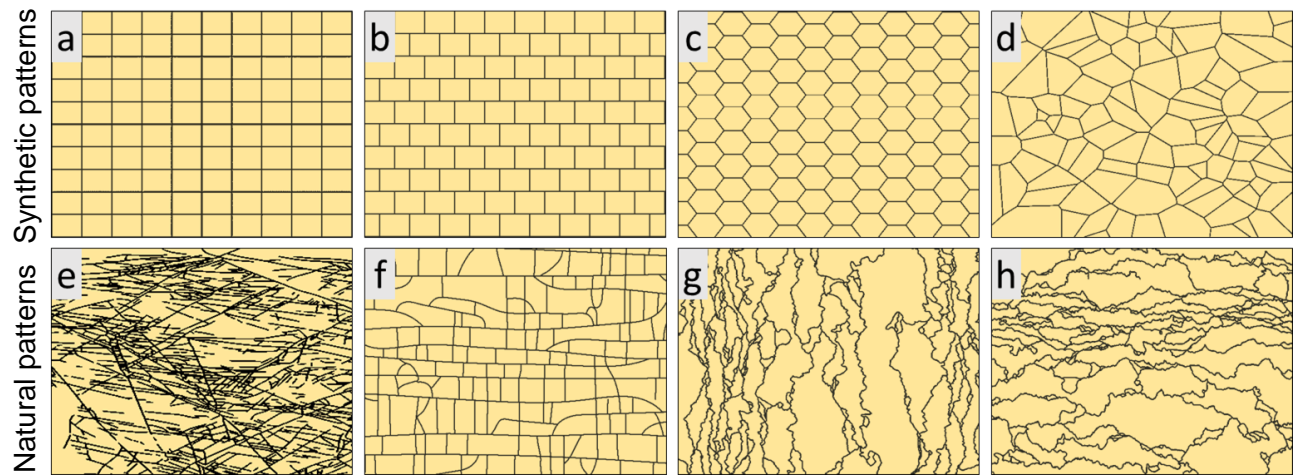


Figure 2. Examples of synthetic and natural rock patterns used in the simulations. The upper row represents synthetic rock textures of a grid (a), brick-wall (b), honeycomb (c) and realistic polycrystalline rock (Voronoi, d). The lower row is our model representation for natural rock images of diagonal cracks (e), orthogonal cracks (f), perpendicular stylolites (g), and parallel stylolites (h).

Figure 3.

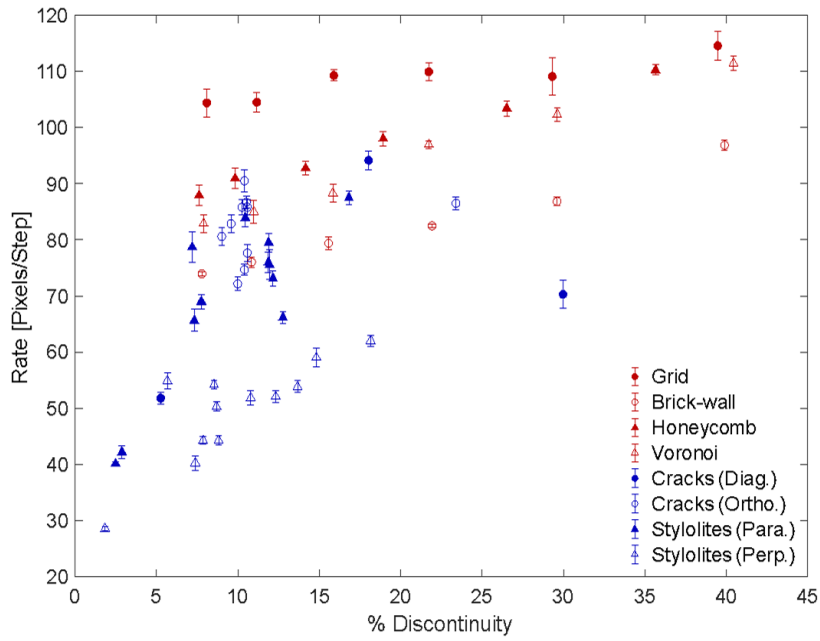


Figure 3. Weathering rate as a function of discontinuity density in synthetic (red) and natural (blue) patterns. Each of the synthetic patterns shows a linear increase in weathering rate with the density of discontinuities. In the natural rock patterns, the trend is less clear. At lower discontinuity density, the weathering rate exhibits a strong dependence on the pattern.

Figure 4.

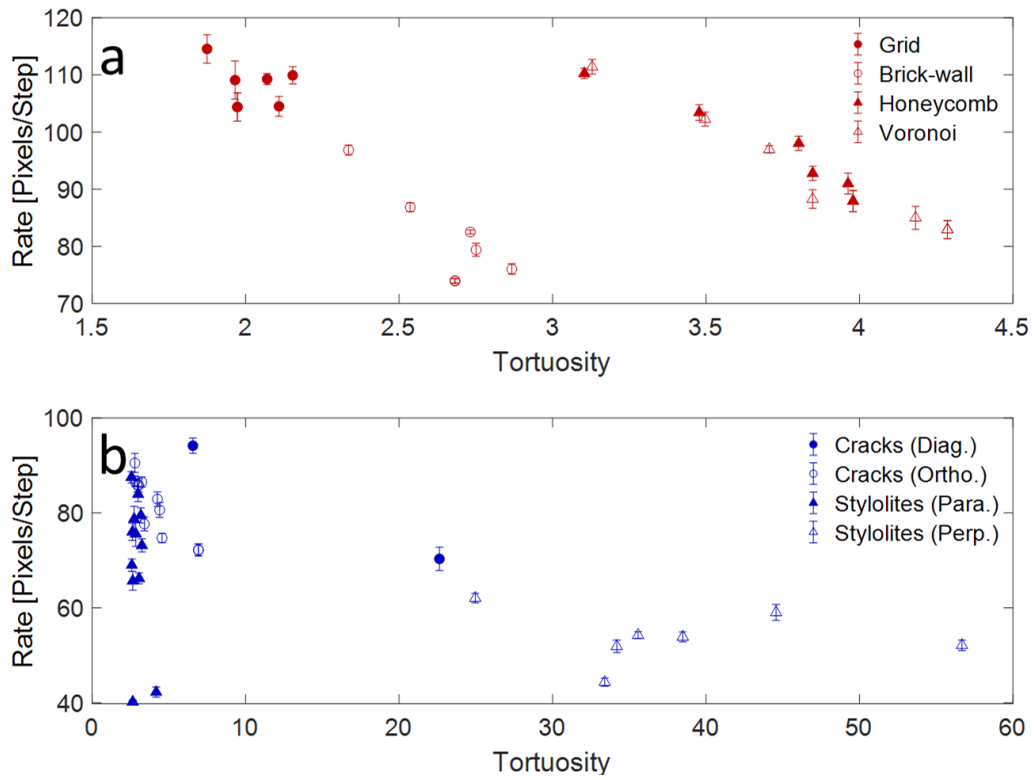


Figure 4. Weathering rate as a function of tortuosity in (a) synthetic patterns and (b) and natural patterns. In the synthetic patterns there are two distinct groups. In the synthetic patterns, there are two distinct trends, in contrast to the natural patterns, which show no clear relationship.

Figure 5.

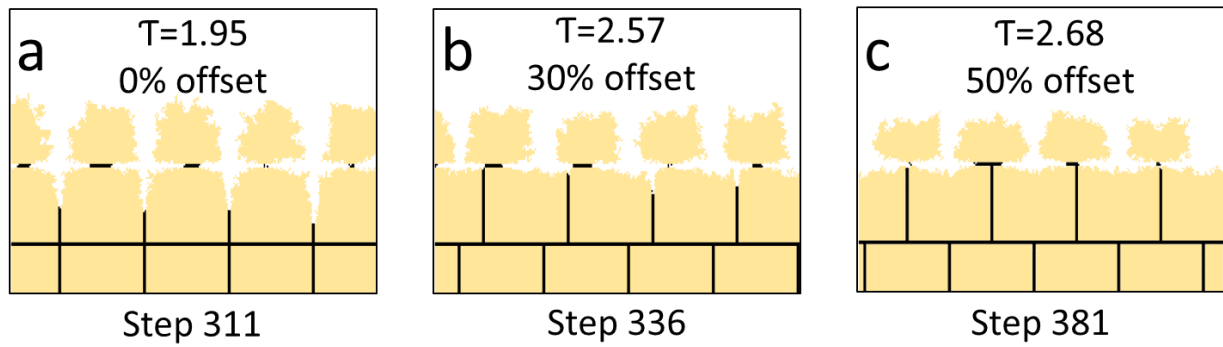


Figure 5. Snapshots of 3 simulations with different offsets and tortuosities. Each image shows the times step directly preceding a grain detachment event. The initial grain size is  $\mu_0=2160$  pixels. Note the decrease in size of detached grains and in the difference in patterns of penetration of the reactive fluid into the rock. In addition, for the lowest level tortuosity the reaction front advances much more rapidly than at higher levels of tortuosity.

Figure 6.

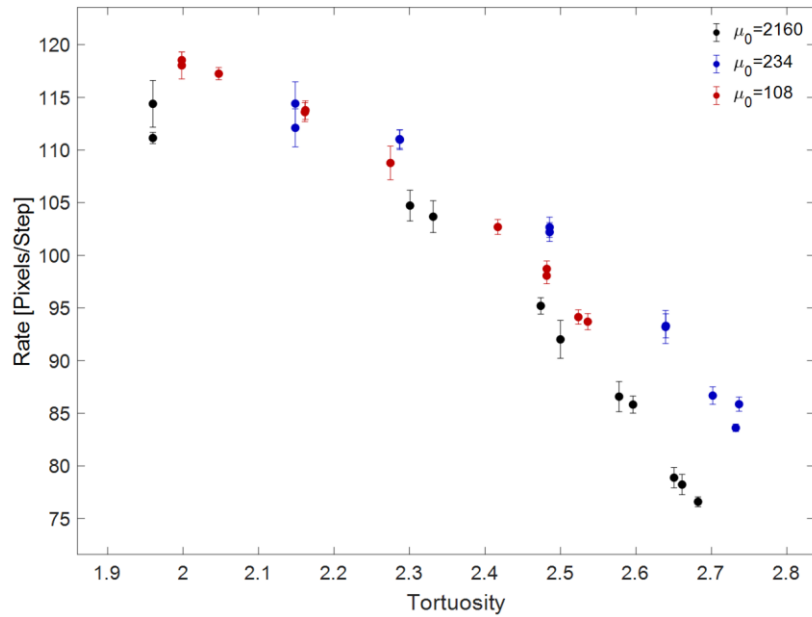


Figure 6. Weathering rate versus tortuosity in simulations with offset from grid (0% offset) to brick-wall (50% offset) and back to grid (100% offset), in three decreasing initial grain sizes  $\mu_0=2160$  pixels (black),  $\mu_0=234$  pixels (blue) and  $\mu_0=108$  pixels (red).

Figure 7.

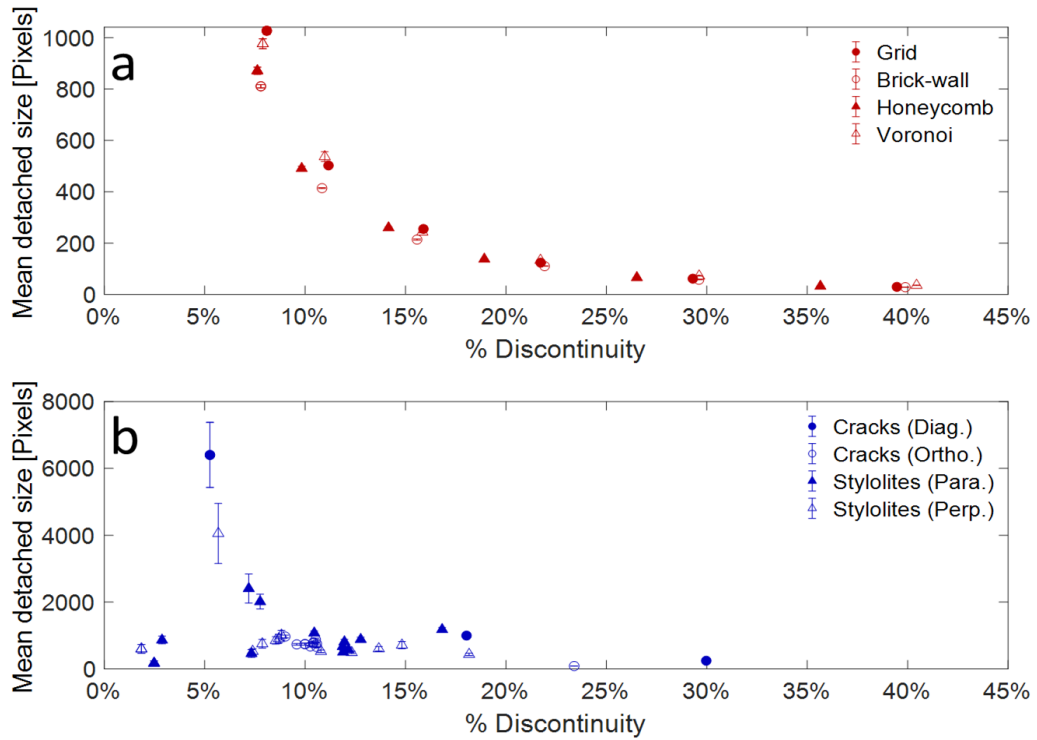


Figure 7. Impact of discontinuity density on mean detachment size in (a) synthetic and (b) natural patterns. The synthetic patterns show a non-linear reduction in detachment grain size with increasing discontinuity density. In the natural patterns, the discontinuity abundance is less systematic, but the trend is similar.

Figure 8.

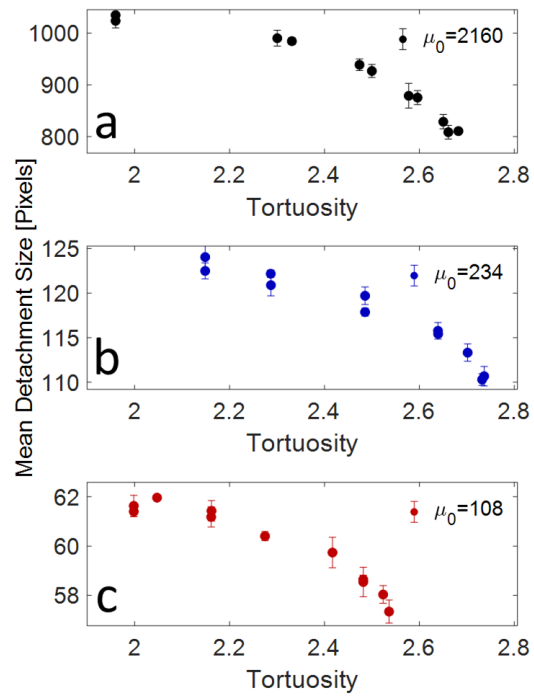


Figure 8. Mean detachment size as a function tortuosity in offset simulations for 3 initial grain sizes pixels (a) 2160 pixels; (b) 234 pixels; and (c) 108 pixels.

Figure 9.

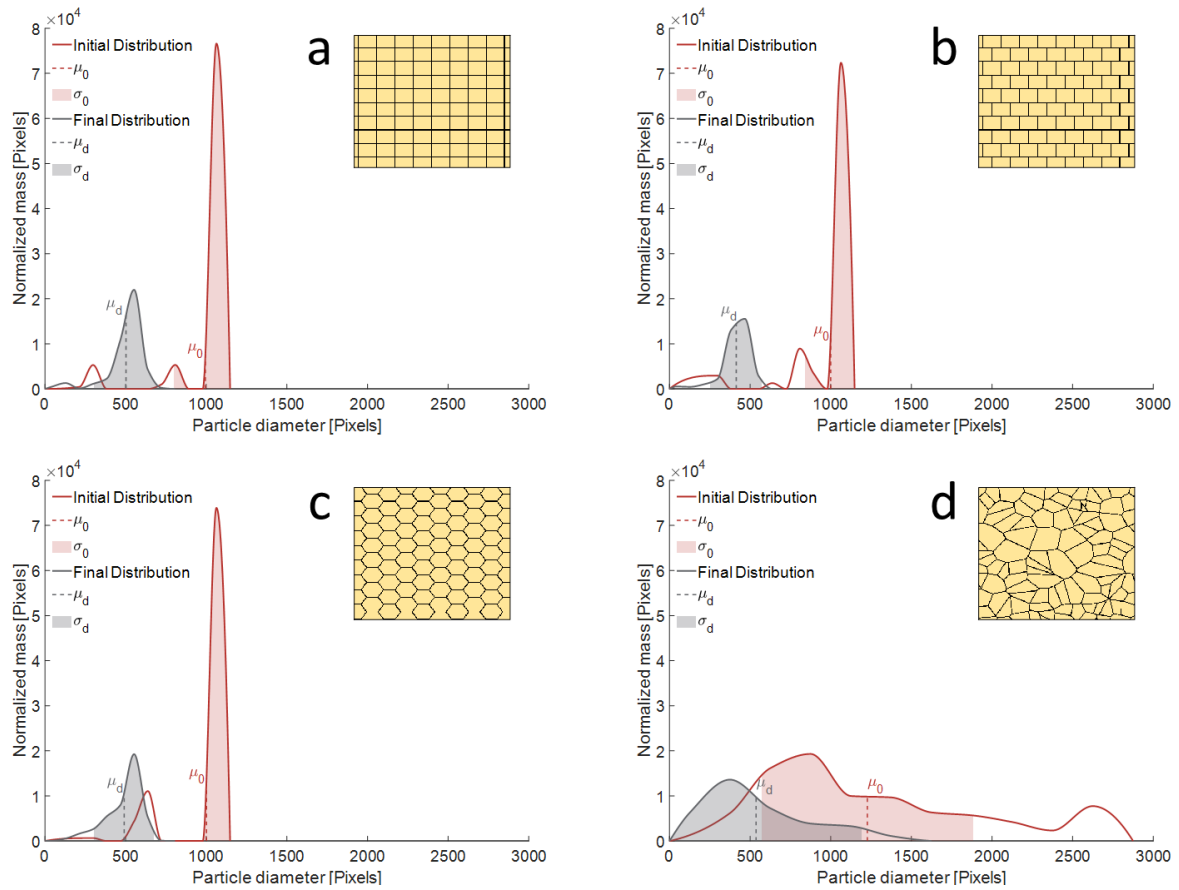


Figure 9. Initial grain size distribution and size distribution of detached grains for synthetic rock patterns: (a) grid; (b) brick-wall; (c) honeycomb; and (d) Voronoi patterns. The initial distribution is shown by the solid red line, with the mean initial grain size indicated by the dashed red line. The standard deviation from the mean is shown by the shaded region. The size distribution of the detached grains is indicated by the solid gray line. The mean detached grain size is shown by the dashed gray line, and the standard deviation from the mean is indicated by the area shaded in gray.

Figure 10.

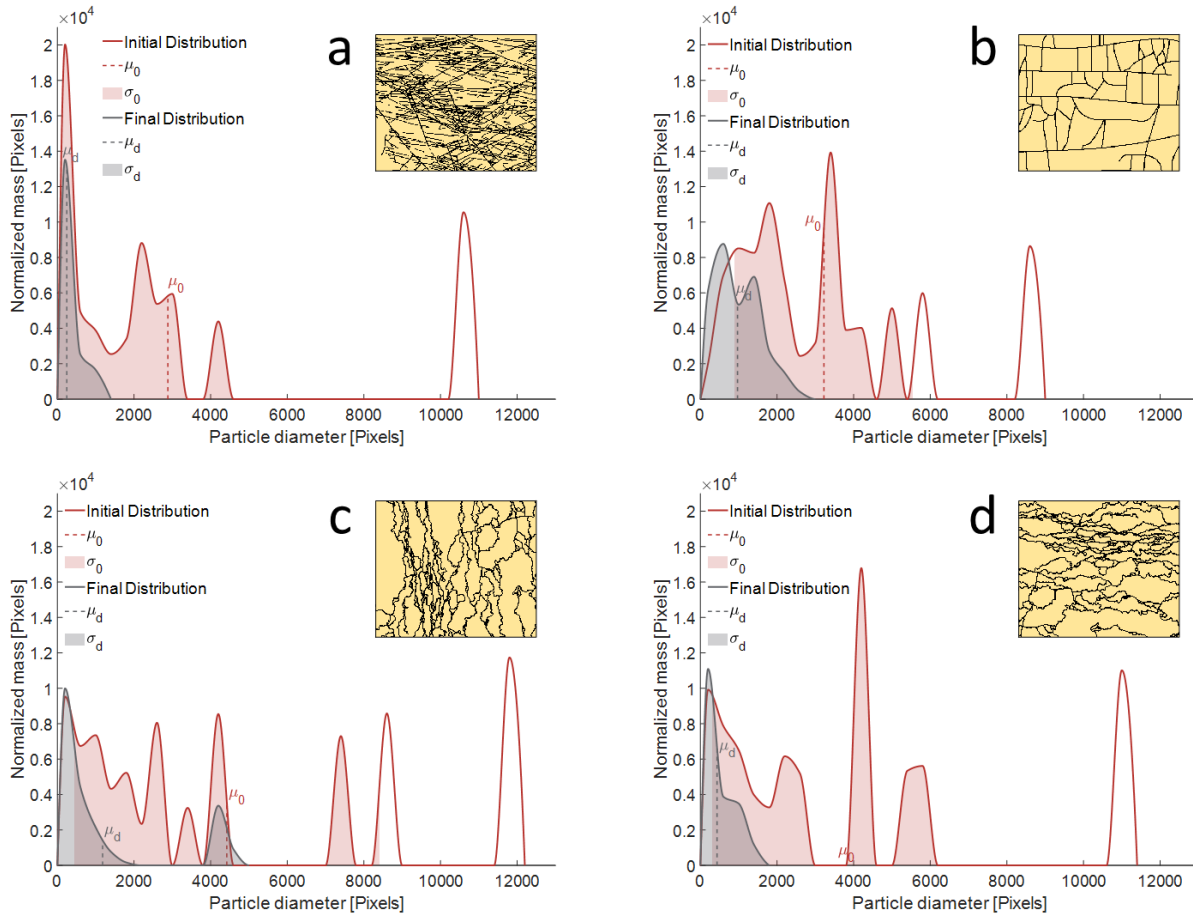


Figure 10. Initial grain size distribution and size distribution of detached grains for natural rock patterns: (a) diagonal cracks; (b) orthogonal cracks; (c) perpendicular stylolites; and (d) and parallel stylolites. The initial distribution is shown by the solid red line, with the mean initial grain size indicated by the dashed red line. The standard deviation from the mean is shown by the pink shaded region. The size distribution of the detached grains is indicated by the solid gray line. The mean detached grain size is shown by the dashed gray line, and the standard deviation from the mean is indicated by the area shaded in gray. The weathering process decreases the modality of the distribution in all tested natural patterns.